

## MIT Open Access Articles

*Precision pH Sensor Based on WO<sub>3</sub> Nanofiber-Polymer Composites and Differential Amplification*

The MIT Faculty has made this article openly available. **Please share** how this access benefits you. Your story matters.

**Citation:** Choi, Seon-Jin et al. "Precision pH Sensor Based on WO<sub>3</sub> Nanofiber-Polymer Composites and Differential Amplification." ACS Sensors 4, 10 (October 2019): 2593–2598 © 2019 American Chemical Society

**As Published:** <http://dx.doi.org/10.1021/acssensors.9b01579>

**Publisher:** American Chemical Society (ACS)

**Persistent URL:** <https://hdl.handle.net/1721.1/128142>

**Version:** Author's final manuscript: final author's manuscript post peer review, without publisher's formatting or copy editing

**Terms of Use:** Article is made available in accordance with the publisher's policy and may be subject to US copyright law. Please refer to the publisher's site for terms of use.



# Precision pH Sensor based on WO<sub>3</sub> Nanofiber-Polymer Composites and Differential Amplification.

Seon-Jin Choi,<sup>§</sup> Suchol Savagatrup,<sup>‡,§</sup> Yoonseob Kim,<sup>‡,§</sup> Jeffrey H. Lang,<sup>||,\*</sup> and Timothy M. Swager,<sup>‡,§,\*</sup>

<sup>§</sup>Department of Chemistry, Massachusetts Institute of Technology, Cambridge, Massachusetts 02139, United States

<sup>‡</sup>Institute for Soldier Nanotechnologies, Massachusetts Institute of Technology, Cambridge, Massachusetts 02139, United States

<sup>||</sup>Electrical Engineering and Computer Science, Massachusetts Institute of Technology, Cambridge, Massachusetts 02139, United States

**KEYWORDS:** WO<sub>3</sub> nanofiber, porous polymer, MOSFET, differential amplifier, pH sensor

**ABSTRACT:** We report a new type of potentiometric pH sensor with sensitivity exceeding the theoretical Nernstian behavior (−59.1 mV/pH). For the pH-sensitive electrode, 1D tungsten oxide (WO<sub>3</sub>) nanofibers (NFs) were prepared to obtain large surface area and high porosity. These NFs were then stabilized in a reactive porous chloromethylated triptycene poly(ether sulfone) (Cl-TPES) binder, to facilitate proton diffusion into the polymer membrane. The measurements were performed with a differential amplifier using matched MOSFETs and providing a 10-fold amplified signal over simple a potentiometric determination. A high pH sensitivity of −377.5 mV/pH and a linearity of 0.9847 were achieved over the pH range of 6.90–8.94. Improved signal-to-noise ratios with large EMF signal changes of 175 mV were obtained in artificial seawater ranging from pH 8.07–7.64 (ΔpH=0.43), which demonstrates practical application for pH monitoring in ocean environments.

Precision determination of solution acidity/alkalinity is widely applicable to environmental, healthcare, and biological technologies.<sup>1-4</sup> For natural systems, the monitoring of pH reveals key information about metabolic states, wound infections, and cell poliferation.<sup>4-6</sup> Since the Industrial Revolution, fossil fuel combustion has produced a significant increase in atmospheric carbon dioxide (CO<sub>2</sub>) that has produced decreases in pH levels in the surface seawater, which is a major environmental concerns.<sup>1</sup> In particular, in addition to warming the planet by absorbing infrared radiation, CO<sub>2</sub> also dissolves to give OH<sub>3</sub><sup>+</sup> and bicarbonate (HCO<sub>3</sub><sup>-</sup>).<sup>7-8</sup> Ocean acidification has impacted numerous marine organisms and shellfish that use calcium carbonate for their structural components are compromised in acidic corrosive seawater.<sup>9</sup>

Potentiometric pH sensors have been widely employed and can be used to make small, cost-effective, and portable sensors.<sup>10</sup> The working principle is to measure the electromotive force (EMF) between a pH sensing electrode and a reference electrode (e.g., Ag/AgCl) in an aqueous environment. The pH responsive electrodes in potentiometric sensors include WO<sub>3</sub>, IrO<sub>2</sub>, RuO<sub>2</sub>, SnO<sub>2</sub>, and Co<sub>3</sub>O<sub>4</sub> as transducers.<sup>11-15</sup> Among these metal oxides, WO<sub>3</sub> has been intensively studied as a pH-sensitive layer as a result of its utility for the facile production into nanostructures, chemical stability, low cost, biocompatibility, and catalytic activity.<sup>16-20</sup> In addition, pH responsive WO<sub>3</sub> exhibited high selectivity against common interfering ions such as Cl<sup>-</sup>, NO<sub>3</sub><sup>-</sup>, SO<sub>4</sub><sup>2-</sup>, F<sup>-</sup>, I<sup>-</sup>, Na<sup>+</sup>, and K<sup>+</sup>. For example, WO<sub>3</sub> nanocolumns,<sup>16</sup> nanoparticles,<sup>21</sup> and nanosheets<sup>22</sup> have been demonstrated high

pH sensitivity. Nevertheless, direct measurement of potentiometric pH responses has the inherent limitation as defined by the Nernst equation, wherein proton coupled redox reactions produce a change of to −59.1 mV/pH unit at room temperature.<sup>23</sup> Several metal oxide pH sensors have been reported that have reached the theoretical maximum in sensitivity with IrO<sub>2</sub> films displaying −59.50 mV/pH,<sup>15</sup> WO<sub>3</sub> nanocolumns having −57.70 mV/pH,<sup>16</sup> and WO<sub>3</sub> nanosheets providing −63.37 mV/pH unit responses.<sup>22</sup> Therefore, there is a need to develop a new type of potentiometric sensing platform to further improve pH outputs that exceed the Nernst-limit voltages. Combining potentiometric sensors with a metal-oxide field-effect transistor (MOSFET) is a promising approach to address this issue. Recent developments in ion-selective FETs (ISFETs) exhibited signal amplification characteristics exceeding theoretical Nernst behavior with dual-gate operation, wherein capacitive coupling between top and bottom gate dielectrics induces significant amplification.<sup>24-27</sup>

Herein, we report sensitive potentiometric pH sensors by making use of MOSFET-based differential amplifiers. A pH-sensitive 1-D nanofibrous tungsten oxide (WO<sub>3</sub>) film creates high surface area and porosity. To stabilize the nanofiber structure, a molecularly porous chloromethylated triptycene poly(ether sulfone) (Cl-TPES) polymeric is added as a reactive permeable binder. A dual N- and P-channel matched MOSFET pair is integrated in the potentiometric two-electrode configuration to give a sensitive pH response (−377.5 mV/pH). This sensitivity value is considerably beyond the theoretical Nernstian value (−59.1 mV/pH). The composite pH sensor with

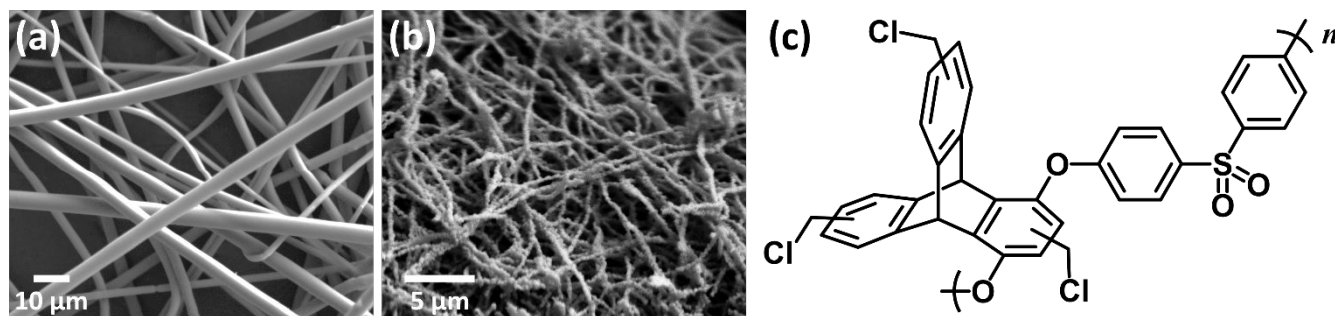
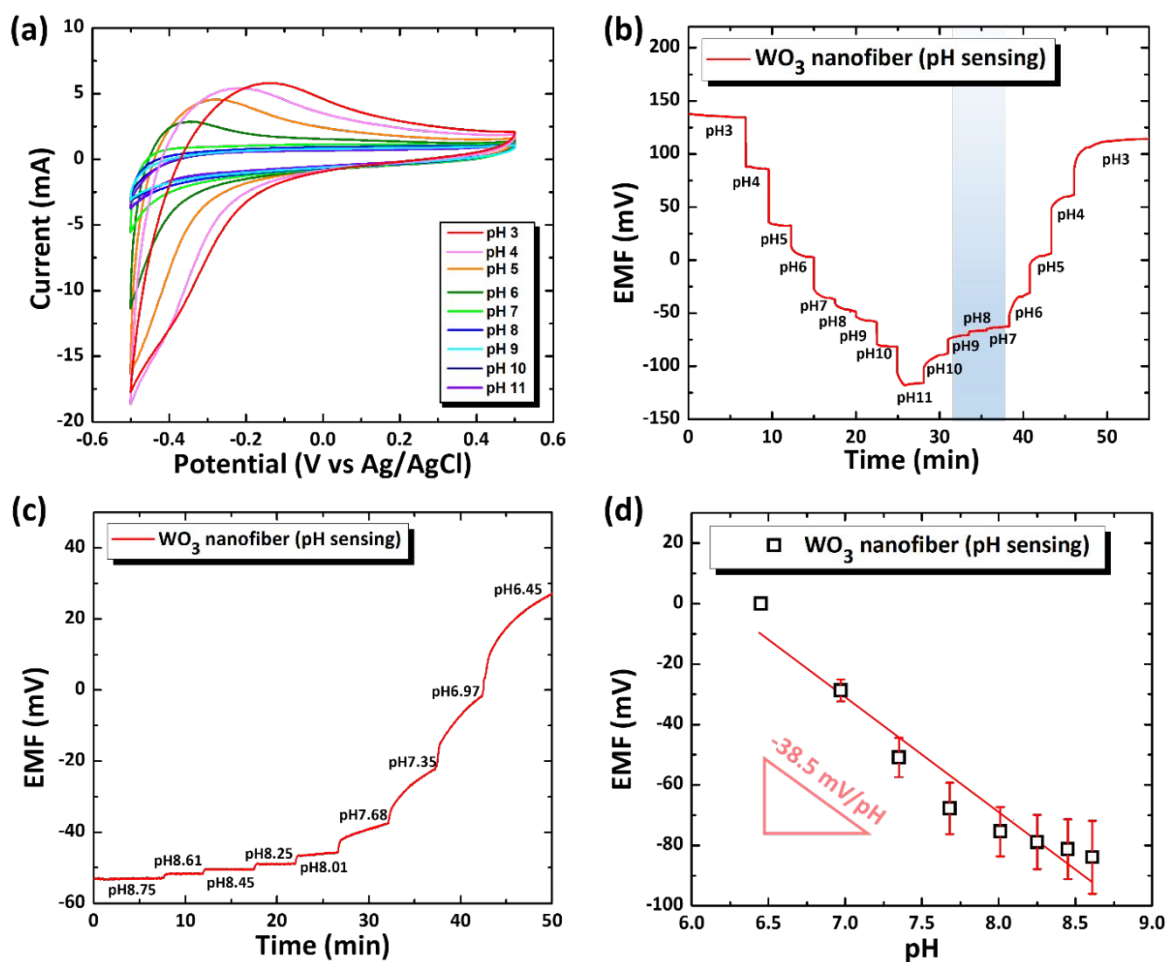


**Figure 1.** SEM images of (a) as-spun PVP/W precursor composite fiber and (b)  $\text{WO}_3$  NFs after calcination. (c) Chemical structure of chloromethylated triptycene poly(ether sulfone) (Cl-TPES).

the differential amplifier can detect trace pH changes to give enhanced potentiometric signal differences ( $\Delta\text{EMF}=34.5$  mV for a  $\Delta\text{pH}=0.05$ ) even in artificial seawater, thereby enabling potential applications for precision monitoring of ocean pH changes.

The pH-responsive  $\text{WO}_3$  nanofibers (NFs) were prepared by an electrospinning process, which creates films with high surface area and porosity.<sup>28-29</sup> Briefly, a composite solution of polyvinylpyrrolidone (PVP)/W precursor  $[(\text{NH}_4)_6\text{H}_2\text{W}_{12}\text{O}_{40} \cdot x\text{H}_2\text{O}]$  was prepared as a dispersion in water. The solution was transferred in a syringe and a high voltage was applied between a syringe nozzle (needle) and an aluminum foil

continuous inorganic  $\text{WO}_3$  NFs structure was obtained (Figure S1) with a roughened surface morphology and reduced fiber diameters of approximately 500 nm (Figure 1b). Mesoscale (2–50  $\mu\text{m}$ ) pores were observed between the  $\text{WO}_3$  NFs, which creates beneficial accessibility of the fibers to the aqueous environment. A triptycene-based porous polymer coating, i.e., Cl-TPES, was applied to the  $\text{WO}_3$  NFs, which is intended to improve the mechanical stability of the sensing electrode. (Figure 1c). Triptycene has a rigid 3D structure with high internal free-volume and mechanical stability, which can provide for stability while not restricting ion diffusion to the surface of the  $\text{WO}_3$  NFs.<sup>30-31</sup>

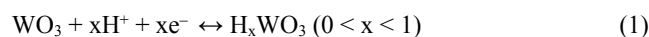


collector for the as-spun PVP/W precursor composite fiber. These fibers display a smooth surface morphology and diameter less than 5  $\mu\text{m}$  (Figure 1a). After calcination at 800  $^\circ\text{C}$ , a

Characteristic cyclic voltammograms of the  $\text{WO}_3$  NFs/Cl-TPES in various pH levels ranging from 3–11 are shown in Figure 2a. The increasing cathodic current below 0 V confirms

**Figure 2.** (a) Cyclic voltammograms of the  $\text{WO}_3$  NFs/Cl-TPES composite vs. Ag/AgCl in the pH range of 3–11 (from  $-0.5$  V to  $0.5$  V with scanning rate of 100 mV/s). Electrochemical potential behavior of the  $\text{WO}_3$  NFs/Cl-TPES composite in the (b) pH 3–11 and (c) pH 6.45–8.75. (d) pH response curve of the  $\text{WO}_3$  NFs/Cl-TPES composite in the pH range of 6.45–8.75.

the intercalation of protons into  $\text{WO}_3$  crystals to form a tungsten bronze ( $\text{H}_x\text{WO}_3$ ) state.<sup>21, 32</sup> In particular, the increased cathodic current and shifts to more positive potential in acidic environment are indicative of conductive  $\text{H}_x\text{WO}_3$  formation. This behavior of the  $\text{WO}_3$  electrode is the basis of the pH response and is described by the following equation<sup>16, 33</sup>:



We did not observe significant differences in cyclic voltammogram behavior of the  $\text{WO}_3$  NFs/Cl-TPES relative to the pristine  $\text{WO}_3$  NFs (Figure S2a), confirming that the Cl-TPES doesn't have intrinsic electrochemical activity and doesn't attenuate the  $\text{WO}_3$  electroactivity. The broad anodic region in the range of  $-0.5\text{V}$ – $-0.4\text{V}$  of the  $\text{WO}_3$  NFs/Cl-TPES compared to the pristine  $\text{WO}_3$  NFs could be an indication of Cl-TPES incorporation with  $\text{WO}_3$  NFs and promoted intercalation of proton into  $\text{WO}_3$  matrix.

Potentiometric sensing was examined from pH 3–11 by measuring EMF signals between the  $\text{WO}_3$  NFs/Cl-TPES layer and an Ag/AgCl reference electrode. Upon changing pH levels the EMF signal changes and then stabilize at a steady-state (Figure 2b). The cyclic pH variations over pH 3–11 demonstrates the reversible pH sensing of  $\text{WO}_3$ /Cl-TPES. We are most interested in pH 6.45–8.75, which has practical

applications such as monitoring chronic wounds dressings (pH 7.4–8.6)<sup>34</sup> and ocean pH monitoring (pH 7.8–8.1).<sup>35</sup> EMF signal changes are observed even with a small pH differences (Figure 2c). However, we observed sensitivity differences depending on the pH scanning direction (Figure 2b) and unstable pH transitions over pH 8 (Figure 2c), which are mainly caused by irreversible reaction in equation (1) as a result of the formation of charge saturation sites in  $\text{WO}_3$  matrix.<sup>21</sup> The calibration curve of EMF over this target pH range reveals a base sensitivity of the  $\text{WO}_3$ /Cl-TPES sensor to be  $-38.5$  mV/pH unit (Figure 2d).

The EMF signals of uncoated pristine  $\text{WO}_3$  NFs were evaluated over the same pH range to investigate the effect of Cl-TPES (Figure S2b-c). Similar to the  $\text{WO}_3$  NFs/Cl-TPES sensor, pristine  $\text{WO}_3$  NFs exhibited large EMF changes in the pH ranges of 3–11 (Figure S2b). EMF signal changes over pH 6.45–8.75 (Figure S2c) revealed a sensitivity of  $-25.6$  mV/pH, which is 66.5% lower than the sensitivity of  $\text{WO}_3$  NFs/Cl-TPES sensor (Figure S2d). This result confirms that the incorporation of Cl-TPES with  $\text{WO}_3$  NFs enhances pH sensitivity.

The theoretical sensitivity of potentiometric pH sensors are intrinsically related to the Nernstian equation<sup>23</sup>:

$$E = E^0 - (2.303R/T/F)\text{pH} = E^0 - 0.05916 \text{ pH} \quad (2)$$

**Table 1.** Comparison of potentiometric sensing performance of  $\text{WO}_3$  NF-based sensors with and without the differential amplifier.

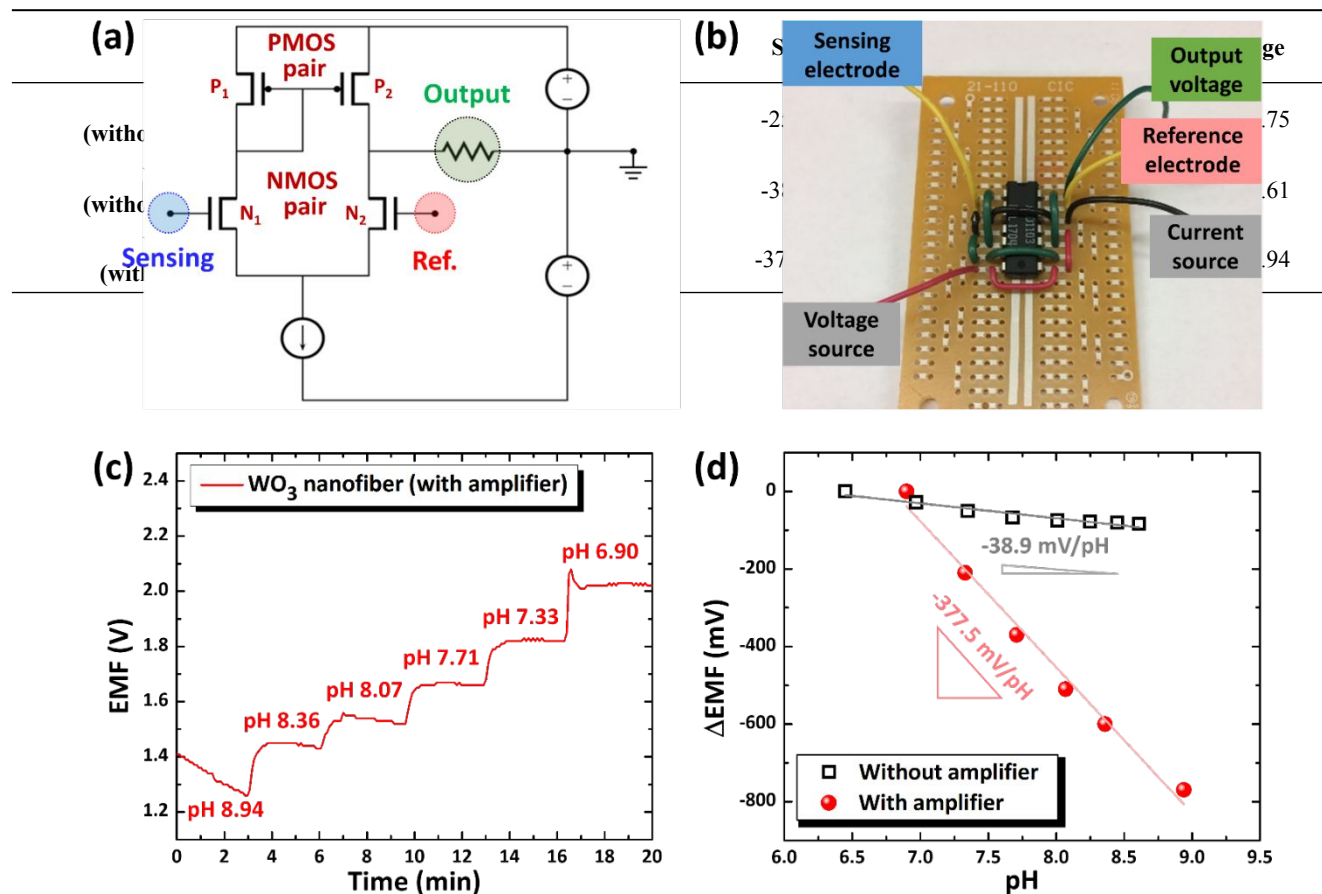


**Figure 3.** (a) Schematic illustration of the circuit design for the potentiometric sensing platform with the differential amplifier. (b) Integration of the differential amplifier on a breadboard with corresponding wire connections. (c) Potentiometric pH sensing using the  $\text{WO}_3$  NFs/Cl-TPES composite with the differential amplifier. (d) pH response curves of the  $\text{WO}_3$  NFs/Cl-TPES composite with and without the differential amplifier.

where  $E_0$  is the standard electrode potential,  $R$  is the gas constant,  $T$  is the temperature, and  $F$  is Faraday's constant. The theoretical maximum sensitivity of a Nernstian proton coupled redox process is thus  $-59.1$  mV/pH at room temperature. To produce a greater voltage output (sensitivity), a signal differential amplifier is combined with the  $\text{WO}_3$  NFs/CI-TPES sensing electrode (Supporting Information). Specifically, we make use of a commercial dual N-channel and dual P-channel matched MOSFET pair (ALD1103, Advanced Linear Device, INC.), wherein the N-channel MOSFETs ( $N_1$  and  $N_2$ ) are connected to form a differential amplifier, with the P-channel MOSFETs ( $P_1$  and  $P_2$ ) serving as a current-mirror load (Figure 3a). The current-mirror load matched P-channel MOSFETs dictate that the currents flowing through  $N_1$ ,  $P_1$ , and  $P_2$  must be the same under the supplied current by the current source. This four-transistor differential amplifier provides a single-ended output current that responds with high gain to the potential difference between the sensing and reference electrodes (Figure 3b and Figure S3). Intrinsic advantages of this amplifier are its stable biasing, and that any external disturbance that affects both transistors will be minimized, thereby providing a method to reduce background signals encountered in complex environments. The potential difference after the gain profited by the differential amplifier is the sensor's output voltage ( $V_{\text{output}}$ ).

To demonstrate the differential amplifier utility, we applied potential differences between the sensing and the reference electrodes using a function generator. An order of magnitude increase in output voltage was observed by the differential amplifier (Figure S4a) and the device faithfully provided a linear amplification (Figure S4b). We also found that the amplification is optimal when the resistance at the output resistor is between  $1$  k $\Omega$  –  $10$  k $\Omega$  and a signal gain of 20 is obtained at  $10$  k $\Omega$ , wherein the experimental gain matches the theoretical value (Supporting Information).

A pH sensor comprising a differential amplifier and a  $\text{WO}_3$  NFs/CI-TPES film was tested over a pH range of 6.90–8.94 (Figure 3c). The output voltages of  $-377.5$  mV/pH is approximately 10 times higher than that obtained without the differential amplifier (Figure 3d and Table 1). In addition, beyond exceeding the typical Nernst-limit ( $-59.1$  mV/pH), this electronically augmented pH sensor displays excellent linearity

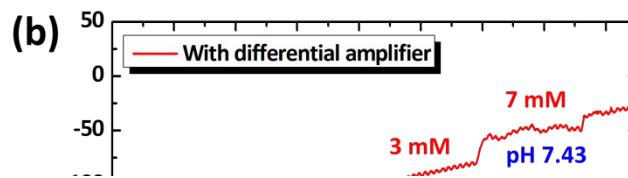
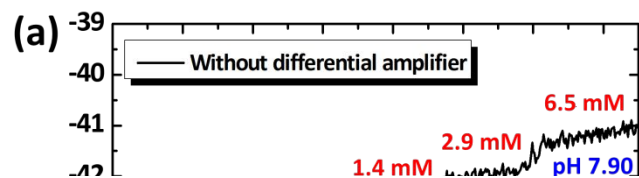
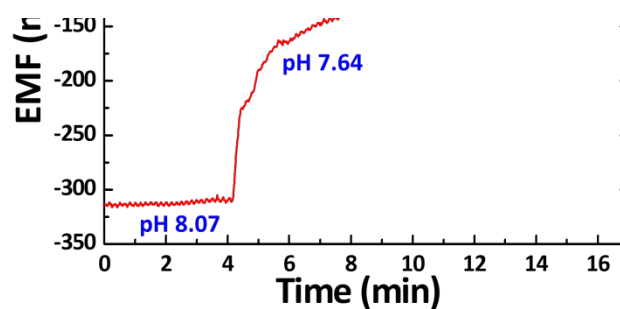
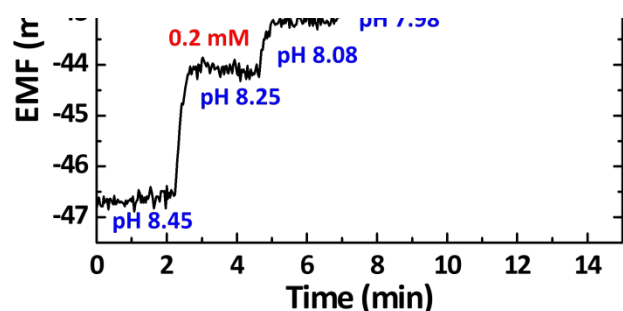


Figure 4. Real-time EMF signals at different pH levels upon subsequent addition of  $\text{HCO}_3^-$  (a) without and (b) with the differential amplifier.



(0.9847).

sensing and monitoring of pH in seawater.

To demonstrate the potential of our amplified pH sensor for monitoring ocean acidification, we prepared artificial seawater, which contained concentrations of  $\text{Na}^+$ ,  $\text{Mg}^{2+}$ ,  $\text{Ca}^{2+}$ ,  $\text{Cl}^-$ , and  $\text{SO}_4^{2-}$ .<sup>36</sup> Solutions of  $\text{NaHCO}_3$  were added sequentially until a concentration of 7 mM in order to simulate ocean acidification. The pH levels were measured as a function of  $\text{NaHCO}_3$  addition using a commercial pH meter, and output voltage was monitored using  $\text{WO}_3$  NFs/CI-TPES sensors (Figure 4). We observed consistent, but small ( $< 3$  mV), signals without the differential amplifier (Figure S5) over pH 8.08 (current pH level in the ocean) to pH 7.90 (projected pH level for 2100) (Figure 4a).<sup>35</sup> In comparison, over the same range the differential amplifier enhanced sensor produced a 175 mV output with a dramatically enhanced signal-to-noise ratios (Figure 4b). A relatively large voltage signal of 34.5 mV was obtained over the narrow pH range from 7.43–7.48 ( $\Delta\text{pH}=0.05$ ). Based on this response we assert that this differential amplifier sensor scheme is promising for portable and low-cost applications for the monitoring of ocean acidification.

We have developed a potentiometric sensing platform that displays voltage sensitivity far beyond theoretical Nernstian behavior. Electrospinning was employed to obtain nanofibrous  $\text{WO}_3$  structures with large surface area and high porosity. To further enhance pH sensing performance, CI-TPES overcoatings are incorporated that have intrinsic free-volume allowing diffusion to the  $\text{WO}_3$  surface. As a result, high pH sensing performance is achieved using the  $\text{WO}_3$  NFs/CI-TPES with a base sensitivity of  $-38.9$  mV/pH as compared to  $-25.6$  mV/pH for the uncoated pristine  $\text{WO}_3$  NFs. Differential amplifiers comprising dual N-channel and dual P-channel matched MOSFET pairs enhance pH sensitivity by increasing the signal-to-noise ratio. Very high sensitivities of  $-377.5$  mV/pH and linearity of 0.9847 are achieved over the pH range of 6.90–8.94, which represents a 6.4-fold improved sensitivity over the theoretical Nernst-limit. The sensing platform is shown to be appropriate for monitoring ocean acidification through experiments wherein bicarbonate ( $\text{HCO}_3^-$ ) is added to artificial seawater. These studies reveal voltage outputs of 175 mV with trace pH changes ranging from 8.07 to 7.64 ( $\Delta\text{pH}=0.43$ ). Future investigations need to be performed by controlling the ratio of  $\text{WO}_3$  NFs and CI-TPES to confirm mechanical stability and long-term stability of the composite for reproducible pH



## ASSOCIATED CONTENT

**Supporting Information.** General materials, synthesis procedures, characterization, signal differential amplifier, additional analysis data. This material is available free of charge via the Internet at <http://pubs.acs.org>.

## AUTHOR INFORMATION

### Corresponding Author

\*E-mail: [tswager@mit.edu](mailto:tswager@mit.edu)

\*E-mail: [lang@mit.edu](mailto:lang@mit.edu)

### Notes

The authors declare no competing financial interest.

## ACKNOWLEDGMENT

This research was supported by the MIT Sea Grant program (2017-R/RCM-50) administered through the United States National Oceanic and Atmospheric Administration.

## REFERENCES

- Staudinger, C.; Strobl, M.; Breininger, J.; Klimant, I.; Borisov, S. M. Fast and stable optical pH sensor materials for oceanographic applications. *Sens. Actuators B* **2019**, *282*, 204-217.
- Gao, W.; Emaminejad, S.; Nyein, H. Y. Y.; Challa, S.; Chen, K. V.; Peck, A.; Fahad, H. M.; Ota, H.; Shiraki, H.; Kiriya, D.; Lien, D. H.; Brooks, G. A.; Davis, R. W.; Javey, A. Fully integrated wearable sensor arrays for multiplexed in situ perspiration analysis. *Nature* **2016**, *529* (7587), 509-514.
- Goh, G. L.; Agarwala, S.; Tan, Y. J.; Yeong, W. Y. A low cost and flexible carbon nanotube pH sensor fabricated using aerosol jet technology for live cell applications. *Sens. Actuators B* **2018**, *260*, 227-235.
- Nyein, H. Y. Y.; Gao, W.; Shahpar, Z.; Emaminejad, S.; Challa, S.; Chen, K.; Fahad, H. M.; Tai, L. C.; Ota, H.; Davis, R. W.; Javey, A. A Wearable Electrochemical Platform for Noninvasive Simultaneous Monitoring of  $\text{Ca}^{2+}$  and pH. *ACS Nano* **2016**, *10* (7), 7216-7224.
- Tamayol, A.; Akbari, M.; Zilberman, Y.; Comotto, M.; Llesha, E.; Serex, L.; Bagherifard, S.; Chen, Y.; Fu, G. Q.; Ameri, S. K.; Ruan, W. T.; Miller, E. L.; Dokmeci, M. R.; Sonkusale, S.; Khademhosseini, A. Flexible pH-Sensing Hydrogel Fibers for Epidermal Applications. *Adv. Healthc. Mater.* **2016**, *5* (6), 711-719.
- Shangguan, J. F.; He, D. G.; He, X. X.; Wang, K. M.; Xu, F. Z.; Liu, J. Q.; Tang, J. L.; Yang, X.; Huang, J. Label-Free Carbon-Dots-Based Ratiometric Fluorescence pH Nanoprobes for Intracellular pH Sensing. *Anal. Chem.* **2016**, *88* (15), 7837-7843.
- Doney, S. C.; Fabry, V. J.; Feely, R. A.; Kleypas, J. A. Ocean Acidification: The Other  $\text{CO}_2$  Problem. *Annu. Rev. Mar. Sci.* **2009**, *1*, 169-192.
- Orr, J. C.; Fabry, V. J.; Aumont, O.; Bopp, L.; Doney, S. C.; Feely, R. A.; Gnanadesikan, A.; Gruber, N.; Ishida, A.; Joos, F.; Key, R. M.; Lindsay, K.; Maier-Reimer, E.; Matear, R.; Monfray, P.; Mouchet, A.; Najjar, R. G.; Plattner, G. K.; Rodgers, K. B.; Sabine, C. L.; Sarmiento, J. L.; Schlitzer, R.; Slater, R. D.; Totterdell, I. J.; Weirig, M. F.; Yamanaka, Y.; Yool, A. Anthropogenic ocean acidification over the twenty-first century and its impact on calcifying organisms. *Nature* **2005**, *437* (7059), 681-686.
- Dore, J. E.; Lukas, R.; Sadler, D. W.; Church, M. J.; Karl, D. M. Physical and biogeochemical modulation of ocean acidification in the central North Pacific. *P. Natl. Acad. Sci. USA* **2009**, *106* (30), 12235-12240.
- Bakker, E.; Pretsch, E. Modern Potentiometry. *Angew. Chem. Int. Ed.* **2007**, *46* (30), 5660-5668.
- Li, Q. W.; Luo, G. A.; Shu, Y. Q. Response of nanosized cobalt oxide electrodes as pH sensors. *Anal. Chim. Acta* **2000**, *409* (1-2), 137-142.
- Lale, A.; Tsopele, A.; Civelas, A.; Salvagnac, L.; Launay, J.; Temple-Boyer, P. Integration of tungsten layers for the mass fabrication of  $\text{WO}_3$ -based pH-sensitive potentiometric microsensors. *Sens. Actuators B* **2015**, *206*, 152-158.
- Fu, Y. M.; Pan, J. C.; Tsou, K. L.; Cheng, Y. T. A Flexible  $\text{WO}_3$ -Based pH Sensor Array for 2-D pH Monitoring Using CPLoP Technique. *IEEE Electr. Device Lett.* **2018**, *39* (6), 881-884.
- Lonsdale, W.; Maurya, D. K.; Wajrak, M.; Tay, C. Y.; Marshall, B. J.; Alameh, K. Rapid measurement of urease activity using a potentiometric  $\text{RuO}_2$  pH sensor for detection of *Helicobacter pylori*. *Sens. Actuators B* **2017**, *242*, 1305-1308.
- Kim, T. Y.; Yang, S. Fabrication method and characterization of electrodeposited and heat-treated iridium oxide films for pH sensing. *Sens. Actuators B* **2014**, *196*, 31-38.
- Salazar, P.; Garcia-Garcia, F. J.; Yubero, F.; Gil-Rostra, J.; Gonzalez-Elipse, A. R. Characterization and application of a new pH sensor based on magnetron sputtered porous  $\text{WO}_3$  thin films deposited at oblique angles. *Electrochim. Acta* **2016**, *193*, 24-31.
- Yuan, S. J.; He, H.; Sheng, G. P.; Chen, J. J.; Tong, Z. H.; Cheng, Y. Y.; Li, W. W.; Lin, Z. Q.; Zhang, F.; Yu, H. Q. A Photometric High-Throughput Method for Identification of Electrochemically Active Bacteria Using a  $\text{WO}_3$  Nanocluster Probe. *Sci. Rep.* **2013**, *3*, 1315. DOI:10.1038/srep01315.
- Kim, S. J.; Choi, S. J.; Jang, J. S.; Kim, N. H.; Hakim, M.; Tuller, H. L.; Kim, I. D. Mesoporous  $\text{WO}_3$  Nanofibers with Protein-Templated Nanoscale Catalysts for Detection of Trace Biomarkers in Exhaled Breath. *ACS Nano* **2016**, *10* (6), 5891-5899.
- Choi, S. J.; Choi, C.; Kim, S. J.; Cho, H. J.; Hakim, M.; Jeon, S.; Kim, I. D. Highly Efficient Electronic Sensitization of Non-oxidized Graphene Flakes on Controlled Pore-loaded  $\text{WO}_3$  Nanofibers for Selective Detection of  $\text{H}_2\text{S}$  Molecules. *Sci. Rep.* **2015**, *5*, 8067. DOI:10.1038/srep08067.
- Mardare, C. C.; Hassel, A. W. Review on the Versatility of Tungsten Oxide Coatings. *Phys. Status Solidi A* **2019**, *216* (12), 1900047. DOI: 10.1002/pssa.201900047.
- Santos, L.; Neto, J. P.; Crespo, A.; Nunes, D.; Costa, N.; Fonseca, I. M.; Barquinha, P.; Pereira, L.; Silva, J.; Martins, R.; Fortunato, E.  $\text{WO}_3$  Nanoparticle-Based Conformable pH Sensor. *ACS Appl. Mater. Interfaces* **2014**, *6* (15), 12226-12234.
- Kuo, C. Y.; Wang, S. J.; Ko, R. M.; Tseng, H. H. Super-Nernstian pH sensors based on  $\text{WO}_3$  nanosheets. *Jpn. J. Appl. Phys.* **2018**, *57* (4), 04FM09. DOI: 10.7567/JJAP.57.04FM09.
- Qin, Y. H.; Kwon, H. J.; Howlader, M. M. R.; Deen, M. J. Microfabricated electrochemical pH and free chlorine sensors for water quality monitoring: recent advances and research challenges. *RSC Adv.* **2015**, *5* (85), 69086-69109.
- Lee, I. K.; Jeun, M.; Jang, H. J.; Cho, W. J.; Lee, K. H. A self-amplified transistor immunosensor under dual gate operation:

- highly sensitive detection of hepatitis B surface antigen. *Nanoscale* **2015**, *7* (40), 16789-16797.
- (25) Lee, I. K.; Lee, K. H.; Lee, S.; Cho, W. J. Microwave Annealing Effect for Highly Reliable Biosensor: Dual-Gate Ion-Sensitive Field-Effect Transistor Using Amorphous InGaZnO Thin-Film Transistor. *ACS Appl. Mater. Interfaces* **2014**, *6* (24), 22680-22686.
- (26) Liu, N.; Liu, Y. H.; Feng, P.; Zhu, L. Q.; Shi, Y.; Wan, Q. Enhancing the pH sensitivity by laterally synergic modulation in dual-gate electric-double-layer transistors. *Appl. Phys. Lett.* **2015**, *106* (7), 073507. DOI:10.1063/1.4913445.
- (27) Jang, H. J.; Cho, W. J. Performance Enhancement of Capacitive-Coupling Dual-gate Ion-Sensitive Field-Effect Transistor in Ultra-Thin-Body. *Sci. Rep.* **2014**, *4*, 5284. DOI: 10.1038/srep05284.
- (28) Kim, S. J.; Choi, S. J.; Jang, J. S.; Cho, H. J.; Kima, I. D. Innovative Nanosensor for Disease Diagnosis. *Acc. Chem. Res.* **2017**, *50* (7), 1587-1596.
- (29) Choi, S. J.; Kim, S. J.; Cho, H. J.; Jang, J. S.; Lin, Y. M.; Tuller, H. L.; Rutledge, G. C.; Kim, I. D. WO<sub>3</sub> Nanofiber-Based Biomarker Detectors Enabled by Protein-Encapsulated Catalyst Self-Assembled on Polystyrene Colloid Templates. *Small* **2016**, *12* (7), 911-920.
- (30) Kim, Y.; Moh, L. C. H.; Swager, T. M. Anion Exchange Membranes: Enhancement by Addition of Unfunctionalized Triptycene Poly(Ether Sulfone)s. *ACS Appl. Mater. Interfaces* **2017**, *9* (49), 42409-42414.
- (31) Swager, T. M. Iptycenes in the design of high performance polymers. *Acc. Chem. Res.* **2008**, *41* (9), 1181-1189.
- (32) Gomis-Berenguer, A.; Iniesta, J.; Fermín, D.; Ania, C. Photoelectrochemical Response of WO<sub>3</sub>/Nanoporous Carbon Anodes for Photocatalytic Water Oxidation. *C* **2018**, *4* (3), 45. DOI:10.3390/c4030045.
- (33) Fenster, C.; Smith, A. J.; Abts, A.; Milenkovic, S.; Hassel, A. W. Single tungsten nanowires as pH sensitive electrodes. *Electrochem. Commun.* **2008**, *10* (8), 1125-1128.
- (34) Ochoa, M.; Rahimi, R.; Ziaie, B. Flexible sensors for chronic wound management. *IEEE Rev. Biomed. Eng.* **2014**, *7*, 73-86.
- (35) Meyers, M. T.; Cochlan, W. P.; Carpenter, E. J.; Kimmerer, W. J. Effect of ocean acidification on the nutritional quality of marine phytoplankton for copepod reproduction. *Plos One* **2019**, *14* (5), 1-22.
- (36) Wilt, F. H.; Benson, S. C. Isolation and culture of micromeres and primary mesenchyme cells. *Method. Cell Biol.* **2004**, *74*, 273-285.

ToC

